

## Calibration and Validation of Phase One Industrial Cameras

Richard Ladstädter<sup>1</sup>, Karlheinz Gutjahr<sup>1</sup>, Roland Perko<sup>1</sup>, Helmut Woschitz<sup>2</sup>

<sup>1</sup> JOANNEUM RESEARCH, Institute DIGITAL, Dept. for Remote Sensing and Geoinformation, Steyrergasse 17, Graz, Austria – {richard.ladstaedter, karlheinz.gutjahr, roland.perko}@joanneum.at

<sup>2</sup> Institute of Engineering Geodesy and Measurement Systems, Graz University of Technology, Austria – helmut.woschitz@tugraz.at

### Commission I

**Keywords:** Camera, Geometric Calibration, Validation.

### Abstract

JOANNEUM RESEARCH has reviewed the geometric lab calibration workflow of Phase One A/S, investigating the calibration method from a theoretical point of view, but also by evaluation of an existing calibration project from their new lab in Denver, USA. In addition, two iXM-RS150F reference cameras (50mm and 150mm lens) have been calibrated in the measurement lab of the Institute of Engineering Geodesy and Measurement Systems (IGMS) at Technical University Graz, Austria and results have been compared with the Phase One calibration certificates. Although correctness and quality of the Phase One calibration workflow could be confirmed, small but significant differences exist and can only be explained using various hypothesis e.g. about the influence of different environmental conditions during calibration. As it is not possible from direct comparison to decide which parameter set is the better or even correct one, methods to validate a camera calibration in the lab have been investigated which exist e.g. for acceptance testing of 3D optical measurement systems. It was found that existing methods based on capturing dedicated test bodies using a dense photo network and comparing reconstructed 3D lengths with the calibrated ones cannot be easily transferred to aerial camera systems, especially for longer focal lengths. Therefore, a new lab validation approach has been developed and tested using more available geodetic level rods, LSM matching of the bar code and an algorithm to transfer the length measurement from the image to object space without need for standard 3D point reconstruction.

## 1. Introduction

### 1.1 Motivation

Phase One A/S (PO) is a manufacturer of industrial camera modules and aerial camera systems for the geospatial market. Recently, PO has installed two new lab calibration facilities in Japan and USA (see Figure 1) and has implemented a fully automated calibration workflow supporting all available camera models and lens types (from 50mm up to 150mm).

JOANNEUM RESEARCH (JR) provides photogrammetric software modules for Phase One since almost 10 years (namely solutions for distortion removal, CIR stacking and stitching of multi-camera systems like PAS 280 and PAS Pana). In January 2024, JR has been asked to review the calibration process implemented at PO. Within a funded research project, JR investigated a lab calibration project done by PO and performed independent calibrations in the measurement lab of the Institute of Engineering Geodesy and Measurement Systems (IGMS) at Technical University Graz, Austria.

During this project, it became evident that the comparison of lab calibrations done in different labs and using different software tools is useful but cannot replace a dedicated validation procedure. This has been the motivation to investigate on existing lab validation methods and to think about possible new ones. We have developed such a new method, which is presented in this paper.

### 1.2 Calibration vs. Validation

Camera calibration and validation are closely related but still different tasks, both needed to ensure correct measurements.

Calibration compares measurements of a device (camera) with a given standard and calculates corrections to be applied on the readings. Validation on the other hand is the task to determine if a (usually calibrated) device fulfils the accuracy level needed for photogrammetric products. In this paper, we will only concentrate on geometric calibration and validation methods in a lab environment. However, we are aware that in-flight camera validation cannot be replaced but only complemented by a lab approach.

### 1.3 Related Research and Standards

First, the authors tried to get an overview of research work and standards related to (geometric) digital camera calibration and validation. As described already in (Cramer, 2006), since the involvement of digital aerial cameras, manufacturers implemented their specific lab calibration methods using different facilities, markers, measurement and adjustment tools. Certification by a national authority (as the USGS) was no longer feasible because of the big variety of different sensor technologies and camera designs. Manufacturer therefore started to issue their own calibration “certificate” to the customer without following a specific standard, which was somehow accepted by the market.

(Cramer et al., 2010) gave an excellent overview of the state-of-the-art at that time and mentions the Digital Airborne Camera Quality Assurance Plan from USGS (Stensaas and Lee, 2008). Certification should only be done for a specific sensor type or camera model, individual cameras should only be validated in a test flight over dedicated test sites. In Europe, EuroSDR tried to implement a similar approach within the EuroDAC activity but it was not clear who would be the authorized institution for

validation and certification (see also Cramer, 2008). To the author’s knowledge, such an authority still does not exist.

(Kresse, 2010) announces the development of a new international standard dealing with calibration and validation of remote sensing imagery sensors (ISO/TS 19159-1, 2014). This standard covers lab as well as in-situ calibration and validation. It contains a quite useful section with terms and definitions, e.g. explaining the difference between validation and verification (which checks against specific requirements). However, this standard is quite abstract and does not describe calibration or validation methods in detail.

Performance validation using a test flight over a dedicated test field by evaluating independent checkpoint residuals is especially useful for complex camera systems (consisting of several modules or cones and including a GNSS/IMU navigation subsystem). In a German standard defining the requirements for airborne (and spaceborn) digital cameras (DIN 18740-4, 2025) it is either required to have a valid calibration certificate for a production flight or to validate the camera system over a signalized test field.

Camera validation in a lab is well known for close range optical 3D measurement systems (e.g. for acceptance tests defined by the ISO 10360-13:2021 standard or an early German standard given in (VDI/VDE 2634 Blatt 1, 2002)). Such validation procedures designed for close range cameras are usually not done for aerial camera systems. However, a “calibration validation” as mentioned in (ISO/TS 19159-1, 2014) which only aims to validate a small set of calibration parameters might also be performed in a lab environment. Such a procedure should be designed to work also for tele lenses and without special reference objects (test bodies).

#### 1.4 Structure of the Paper

In the next section, investigations on lab calibration including lab calibrations experiments of PO cameras in Graz are presented. This is followed by a section describing a new camera validation method in a lab, the validation experiments done in the Graz lab and some results for a PO camera with 50mm lens. Please note that the lab calibration experiments as well as first results of the validation experiment have already been presented in an Austrian conference for the German speaking community (Ladstädter et al., 2025). This paper however gives less detail on the calibration topic but focuses more on the new developed validation method. It also provides updated, corrected and extended results as a calculation bug has been fixed and much more images have been evaluated to prove the correctness of the method.

## 2. Lab Calibration Experiments

### 2.1 Evaluation of a Phase One Calibration Project

Lab calibration measurements done by PO for an iXM-RS150F camera equipped with a 150mm lens in the calibration lab in Denver (see Figure 1) have been evaluated using JR photogrammetric tools and compared to the PO result (dated from May, 2024). It is important to note that none of the approximately 2000 coded markers of the 3D test field has given 3D reference coordinates and the calibration room is not temperature stabilized. Therefore, one of the research questions has been if such a test field allows for high quality camera

calibration at all. Theoretical considerations found in literature (Remondino and Fraser, 2005; Luhmann, 2023) as well as empirical tests proved that calibration parameters (for single cameras) are not affected at all by the scale of the test field which can therefore be fixed arbitrarily.



Figure 1. Phase One calibration facility (7m x 3m x 5.4m in width, height, depth) located in Denver, USA.

Table 1 shows the high number of image points (P2D) due to the large number of calibration images taken and available markers (P3D). This results in a large number of observations (Obs) and a high redundancy number (DOF). For the evaluation with our Matlab based adjustment tool “PhoBA” the data set has been significantly reduced to speed up processing (see Table 1, second row).

	#Img	#P2D	#P3D	#Obs.	DOF
PO	180	130488	1592	260963	255097
JR	44	32001	1523	68651	63640

Table 1. Statistics of the PO data set and the reduced JR data set

JR uses the same set of ten Brown-Conradi parameters (Brown, 1971) so that they can directly be compared with the parameters listed in the PO calibration certificate. Parameters are almost identical e.g., deviations of the parameters of the inner orientation are below 1 $\mu$ m (see Table 3 in Ladstädter et al., 2025). As expected, standard deviations of the JR solution are bigger (but still reasonable) due to the reduced measurement data and lower redundancy. Overall, this experiment verifies that exact the same coordinate system and parameter definitions are used.

### 2.2 Calibration of PO Cameras in the Graz Lab

Two PO reference cameras (iXM-RS150F cameras equipped with a 50mm and 150mm lens) have been investigated in the IGMS calibration lab in Graz on May 27<sup>th</sup>, 2024. In contrast to the PO calibration facility, the Graz lab is fully temperature stabilized and all of the 250 calibration markers have precisely known 3D coordinates derived from a geodetic survey. This means that calibration results have been derived not only using different software solutions but in different labs and with a different image acquisition strategy. Table 2 lists the number of calibration images taken first with camera #1 (150mm lens) and then with camera #2 (50mm lens). For both cameras, the same number of images has been taken, using aperture setting F5.6

and F22. At each position (station), images have been taken in four different kappa orientations (0, 90, 180, 270 deg), then the aperture was changed and the same set of images was taken with the new aperture. The number of stations (and thus images) is higher for the 50mm lens as the 150mm lens does not allow to use distances below ~10m but the 50mm lens still works at that distances.

Cam#	Lens	Stations	Image#	D <sub>min</sub>	D <sub>max</sub>
1	150mm	8	36 / 36	11m	35m
2	50mm	10	52 / 52	7m	35m

Table 2. Statistics for the calibration projects in the Graz lab.

More details about image acquisition and evaluation can be found in (Ladstädter et al., 2025). As done for the Denver calibration project, calibration parameters and their estimated standard deviations have been directly compared to those published in the PO calibration certificates dating from May 1<sup>st</sup>, 2024 (see Table 3 and 4, left column).

Param	PO	JR	Unit
c	51.5406 ±0.0001	51.5503 ±0.0006	[mm]
PPA x	0.2127 ±0.0001	0.2041 ±0.0021	[mm]
PPA y	0.0115 ±0.0001	0.0170 ±0.0017	[mm]
K1	1.6e-05 ±2.3e-09	1.7e-05 ±7.2e-08	[mm <sup>-2</sup> ]
K2	-5.7e-09 ±4.8e-12	-6.9e-09 ±1.8e-10	[mm <sup>-4</sup> ]
K3	9.9e-13 ±3.2e-15	1.7e-12 ±1.3e-13	[mm <sup>-6</sup> ]
P1	2.7e-07 ±3.5e-09	8.3e-07 ±2.9e-07	[mm <sup>-1</sup> ]
P2	-2.6e-07 ±2.8e-09	-2.0e-07 ±2.4e-07	[mm <sup>-1</sup> ]
B1	1.2e-05 ±8.3e-08	2.2e-05 ±5.0e-06	[ ]
B2	-6.6e-06 ±8.2e-08	3.8e-06 ±5.1e-06	[ ]

Table 3. Calibration results for the 50mm lens (at F22).

Param	PO	JR	Unit
c	146.321 ±0.0005	146.339 ±0.0055	[mm]
PPA x	0.0907 ±0.0002	0.0933 ±0.0081	[mm]
PPA y	-0.0628 ±0.0002	-0.0640 ±0.0062	[mm]
K1	-2.9e-06 ±1.8e-09	-2.8e-06 ±5.3e-08	[mm <sup>-2</sup> ]
K2	-1.1e-09 ±4.1e-12	-1.5e-09 ±1.1e-10	[mm <sup>-4</sup> ]
K3	7.8e-13 ±2.7e-15	1.0e-12 ±7.8e-14	[mm <sup>-6</sup> ]
P1	2.7e-07 ±5.9e-09	1.1e-07 ±1.3e-07	[mm <sup>-1</sup> ]
P2	1.5e-06 ±4.7e-09	1.7e-06 ±1.0e-07	[mm <sup>-1</sup> ]
B1	-2.3e-05 ±8.5e-08	-1.6e-05 ±2.5e-06	[ ]
B2	1.0e-06 ±8.4e-08	-6.1e-06 ±2.5e-06	[ ]

Table 4. Calibration results for the 150mm lens (at F22).

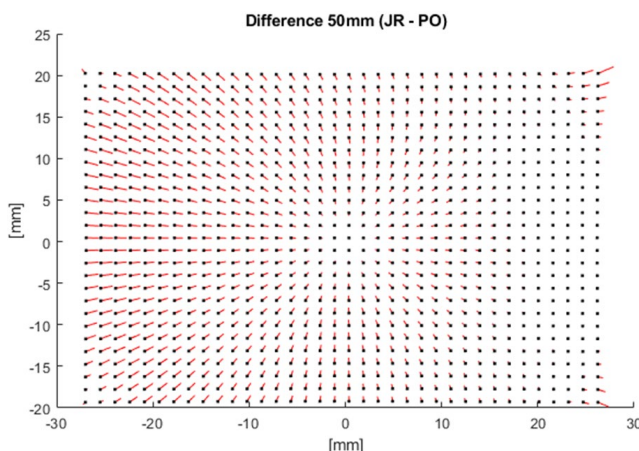


Figure 2. Difference in distortion for the 50mm lens (JR – PO) computed for a regular grid.

To get a better impression about the geometric difference between the PO and JR solution, distortion values have been calculated for a regular grid and subtracted from each other. The difference plot for the 50mm lens is given in Figure 2. The maximum difference vector can be seen in the upper, right corner representing 2.3µm. Please note that the absolute radial distortion reaches more than 100 pixel in the image corners due to the non-balanced radial distortion function, which might cause some problems to model the distortion correctly in the very image corners.

The min/max difference of the distortion grids is -1.6 / +2.3 pixel in *x* and -1.5 / +1.5 pixel in *y*, the RMS of the grid difference is ±0.6 pixel for *x* and ±0.4 pixel for *y* respectively. Please note that until now only the distortion parameters itself have been used in the geometric analysis. Applying a correction scale to compensate for different focal lengths of the 50mm lens (10µm between the JR and PO solutions), the RMS value of the differences calculated on a regular grid dropped down to ±0.3 and ±0.2 pixels for the *x*- and *y*-coordinate, respectively.

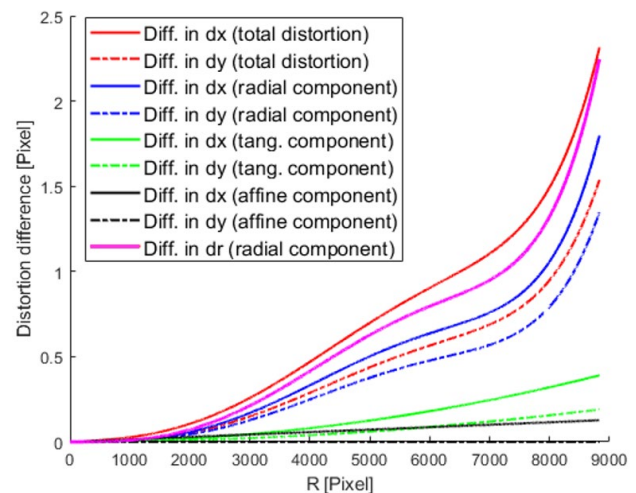


Figure 3. Distortion difference for the 50mm lens (JR – PO).

Another possibility to analyse distortion differences more deeply is to evaluate them along the main image diagonal (e.g. for the upper, right image quadrant). In Figure 3, differences are shown separately for the radial, tangential and affine components and for the *x*- and *y*-coordinate, respectively. The total distortion difference (sum of all components) is plotted as red line (separated for the *x*- and *y*-coordinate). The radial component, usually being the largest component, is also shown as radial correction *dr* (plotted in magenta).

From this Figure it can also be seen that the linear part of the radial distortion (gradient approximately 1.5/9000 pixel = 2e-4) corresponds well to the correction scale applied due to the difference in focal length. One possible explanation for the difference between the JR and PO solutions is the high correlation (about 50%) between the focal length and the radial distortion parameters, which can compensate each other to a certain degree.

It is remarkable that for the 150mm lens the situation is different: There is a significant difference of the focal length (18µm) between the JR and PO solutions but the analysis of the geometric difference caused by the distortion parameters is below 0.2 pixels for most of the image area (see Figure 4). The min/max difference between the distortion grids is -0.44 / 0.15

pixel for the  $x$  component and  $-0.09 / 0.29$  pixel for the  $y$  component with an RMS of only  $\pm 0.06$  and  $\pm 0.05$  pixel respectively. The correlation between the focal length parameter and the radial distortion parameters (below 15%) and the maximum radial distortion (about 30 pixels in the image corners) is much smaller than for the 50mm lens.

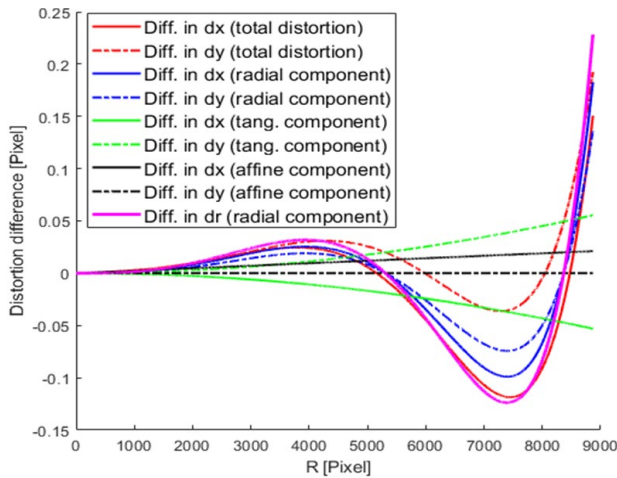


Figure 4. Distortion difference for the 150mm lens (JR – PO).

The difference observed in the focal length parameter can be explained either by a real change of the lens body due to different environmental conditions between the Denver and Graz lab and/or by the different dimensions of the Graz lab, which allows for long distances but has very limited space in across direction. Together with the limited number of calibration images taken in Graz (only 36) the accuracy of the focal length estimation is limited (see Table 4).

The calibration result for both cameras calibrated at aperture F5.6 is given in Table 5 below. Comparison with the parameters of the calibration using aperture F22 (see Tables 3 and 4) shows that there is no significant difference for the 50mm lens. For the 150mm lens, the measurement accuracy is quite bad due to the blurred images using the open aperture, which results in large standard deviations for all parameters. Beginning with parameter K3, parameters are not significant any more.

Param	50mm (JR)	150mm (JR)	Unit
c	51.5490 $\pm$ 0.0007	146.353 $\pm$ 0.0194	[mm]
PPA x	0.2047 $\pm$ 0.0020	0.2538 $\pm$ 0.0285	[mm]
PPA y	0.0166 $\pm$ 0.0016	-0.2067 $\pm$ 0.0224	[mm]
K1	1.6e-05 $\pm$ 7.3e-08	-4.5e-06 $\pm$ 1.8e-07	[mm <sup>-2</sup> ]
K2	-6.6e-09 $\pm$ 1.8e-10	1.5e-09 $\pm$ 4.0e-10	[mm <sup>-4</sup> ]
K3	1.5e-12 $\pm$ 1.3e-13	-6.8e-13 $\pm$ 2.7e-13	[mm <sup>-6</sup> ]
P1	7.5e-07 $\pm$ 2.8e-07	-3.7e-06 $\pm$ 4.8e-07	[mm <sup>-1</sup> ]
P2	-1.8e-07 $\pm$ 2.3e-07	5.3e-06 $\pm$ 3.8e-07	[mm <sup>-1</sup> ]
B1	9.2e-06 $\pm$ 4.8e-06	6.7e-06 $\pm$ 8.9e-06	[ ]
B2	-2.8e-06 $\pm$ 5.0e-06	7.1e-07 $\pm$ 8.9e-06	[ ]

Table 5. Calibration results for aperture F5.6 for both lenses.

Figure 5 shows the quite large radial difference (5.5 pixels) between the F22 and F5.6 solution. However, this effect could not be reproduced outside the lab. After discussions between PO and the lens manufacturer, it turned out that radial distortions can be explained by the 150mm lens design and will only happen for short distances at open aperture for cameras focused to infinity. For object distances larger than 50m, no visible radial distortions are expected.

Please note that direct comparison of calibration results as shown in this section cannot be considered as full validation of a camera calibration but still delivered valuable information for PO.

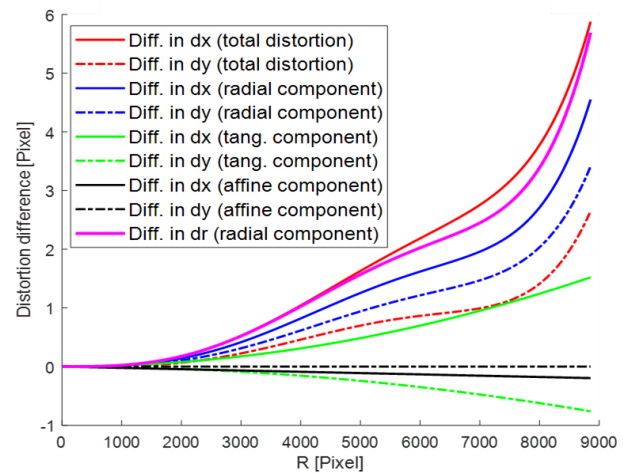


Figure 5. Distortion difference for the 150mm lens (F22–F5.6).

### 3. Lab Validation Experiment

For the authors it would be beneficial to have some simplified validation procedure available, which can be carried out using “standard” equipment available in a measurement lab. Therefore, experiments using Zeiss level rods have been carried out in the Graz lab. The level rods have been installed before the camera calibration in horizontal and vertical orientation on the back wall and on a concrete table separated by about 2m in Z-direction (see Figure 8). Level rods from Zeiss are commonly available and are delivered with a calibration certificate.

#### 3.1 Method

The basic idea is to avoid full 3D reconstruction of reference points by using only 2D image measurements. For that, the 2D distance between the top and bottom reference point measured in the image has to be corrected very precisely for image scale. (Maset and Fusiello, 2024) have derived Formulas to calculate the local image scales for a given image coordinate  $(u, v)$  in both coordinate directions  $(m_u, m_v)$ . From that, a local image scale in direction of the depicted level rod can be calculated in a rectified and oriented image and integrated along the straight line between the top and bottom reference point. This results in a more accurate length measurement as compared with the distance derived from the reconstructed 3D points. This is especially true when only a small baseline can be used due to limited lab space which results in bad intersection of image rays.

##### 3.1.1 Least Squares Matching

The bar code of the Zeiss level rods consists of a sequence of black and white segments very accurately aligned with a cm scale (scale accuracy  $\pm 10$ ppm). We use 10cm long sections on the lower and upper end of the levels and define a bottom and top reference point in the middle of that sections at  $L1=12$ cm and  $L2=292$ cm (see Fig. 6). For these sections, synthetic template images have been generated with dimensions 200 x 50 pixels (and thus a resolution of 0.5mm per pixel). The additional template corner points 0-3 will be used to define the

orientation and scale of the level rod depicted in a calibration image.

A least squares matching (LSM) algorithm including projective parameters (after Bethmann and Luhmann, 2011) has been implemented. LSM allows for very accurate measurements of the Zeiss code at both ends of the level (see Figures 6 and 7) but requires approximate values of high quality for the search position and projective parameters.

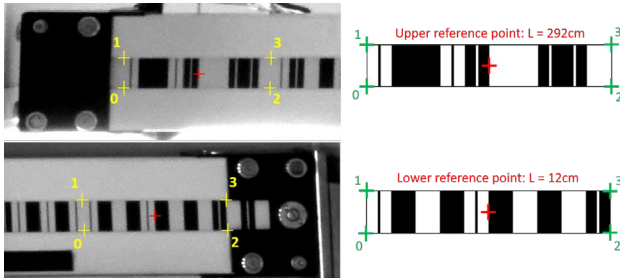


Figure 6. Top and bottom section of the Zeiss 3m level rod and LSM template produced for the bar code.

Figure 7 shows an example of the LSM measurement of the bottom reference point on the vertical level. On the left side the search window and an image crop of 200 x 50 pixels transformed with the initial parameters is shown. This image is compared with the LSM template (shown in the middle) and new position and projective parameters are estimated. After 15 iterations, convergence is reached (final transformed and difference image given on the right side). In this sample, an estimated position accuracy of  $\pm 0.04$  and  $\pm 0.06$  pixels is achieved in column and line direction respectively.

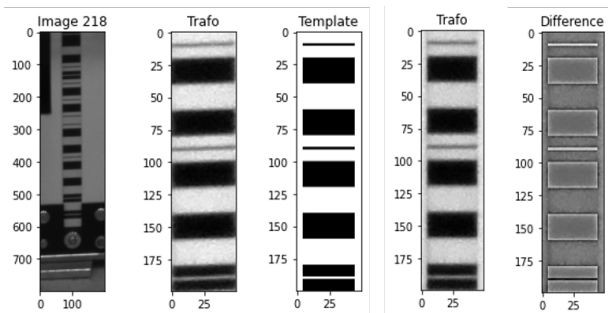


Figure 7. First and last iteration (#15) of a LSM measurement.

### 3.1.2 Local Image Scale Determination and Correction

The 2D distance between the top and bottom reference point measured in the image has to be corrected very precisely for image scale. (Maset and Fusiello, 2024) have derived Formulas to calculate the local image scales for a given image coordinate  $(u,v)$  in both coordinate directions  $(m_u, m_v)$ . We expand their approach in two ways: 1) consider also the kappa angle to derive  $m_u, m_v$  and 2) calculate the image scale  $m_S$  in an arbitrary direction defined by the connection between the reference points in the undistorted image. For that we use the well-known photogrammetric equation to project an image point  $x, y$  into object space and calculate the corresponding  $X, Y$  coordinate for a given (fixed)  $Z$  value (see Equations 1 and 2):

$$X = X_0 - (Z - Z_0) \cdot \frac{r_1^T \cdot \bar{x}}{r_3^T \cdot \bar{x}} = X_0 - H \cdot \frac{f(x,y)}{g(x,y)} \quad (1)$$

$$Y = Y_0 - (Z - Z_0) \cdot \frac{r_2^T \cdot \bar{x}}{r_3^T \cdot \bar{x}} = Y_0 - H \cdot \frac{h(x,y)}{g(x,y)} \quad (2)$$

$$\bar{x} = \begin{pmatrix} x - x_0 \\ y - y_0 \\ -c \end{pmatrix} \quad R = \begin{bmatrix} r_1^T \\ r_2^T \\ r_3^T \end{bmatrix}$$

using

where  $R = R(\omega, \phi, \kappa)$  rotation matrix  
 $c$  = principal distance  
 $x, y$  = image coordinates  
 $X_0, Y_0, Z_0$  = coordinates of projection centre  
 $X, Y, Z$  = object coordinates

With  $H$  being the distance of the camera to a given  $Z=\text{const.}$  plane we can give the total differential of  $X$  and  $Y$  with respect to  $x$  and  $y$  (see Equations 3 to 7):

$$\frac{\partial X}{\partial x} = -H \cdot \left( \frac{R_{11} \cdot g(x,y) - f(x,y) \cdot R_{31}}{g^2(x,y)} \right) \quad (3)$$

$$\frac{\partial X}{\partial y} = -H \cdot \left( \frac{R_{12} \cdot g(x,y) - f(x,y) \cdot R_{32}}{g^2(x,y)} \right) \quad (4)$$

$$\frac{\partial Y}{\partial x} = -H \cdot \left( \frac{R_{21} \cdot g(x,y) - h(x,y) \cdot R_{31}}{g^2(x,y)} \right) \quad (5)$$

$$\frac{\partial Y}{\partial y} = -H \cdot \left( \frac{R_{22} \cdot g(x,y) - h(x,y) \cdot R_{32}}{g^2(x,y)} \right) \quad (6)$$

$$dX = \frac{\partial X}{\partial x} \cdot dx + \frac{\partial X}{\partial y} \cdot dy ; \quad dY = \frac{\partial Y}{\partial x} \cdot dx + \frac{\partial Y}{\partial y} \cdot dy \quad (7)$$

With (7) we can therefore calculate changes of the  $X, Y$  object coordinates caused by small changes of the  $x, y$  coordinate e.g. along a line. For any short line section  $ds$  we can furthermore calculate the corresponding length of the projected line  $dS$  (cf. Formula 8).

$$ds = \sqrt{dx^2 + dy^2} ; \quad dS = \sqrt{dX^2 + dY^2} ; \quad m_S = \frac{dS}{ds} \quad (8)$$

$$L_{2D} = \int_{\bar{x}_1}^{\bar{x}_2} ds \cong \sum_{i=1}^n \Delta s_i(x,y) \quad (9)$$

$$L_{3D} = \int_{\bar{x}_1}^{\bar{x}_2} m_S \cdot ds = \int_{\bar{x}_1}^{\bar{x}_2} dS(dx, dy) \cong \sum_{i=1}^n \Delta S_i(x,y) \quad (10)$$

The local image scale  $m_S$  for a given direction (along the line) can easily be derived by Formula (8). Computing the length  $L_{2D}$  between two points in the image is trivial (9). Finally, the 3D length  $L_{3D}$  of the line between two points  $x_1$  and  $x_2$  is computed with arbitrary accuracy by summation of line segments  $\Delta S$  corresponding to small line segments  $\Delta s$  in the image. From that, a local image scale in direction of the depicted level rod can be calculated in a rectified and oriented image and integrated along the straight line between the top and bottom reference point.

### 3.2 Image Measurements and Evaluation

Calibration images of the PO 50mm/F22 calibration project have been used for efficiency (and thus validation is not strictly independent from the calibration step). In order to ensure quick and correct convergence of the iterative LSM adjustment, coarse measurements of the reference points and the additional corner points of the templates have been done in 16 images for both the vertical and horizontal level rod and thus for distances

between 5.5m and 11m. Due to not optimal illumination, image measurement accuracy degrades quickly for longer distances. For the remaining images, manual measurements of the reference points have been performed (only used for 3D reconstruction).

Table 6 lists the exterior orientation parameters, which are used to set up equations (1) and (2) for each of the 16 selected images. Note that from each position, images have been taken at four different kappa angles using 90 deg rotation steps and therefore the level rods are visible at many different image positions. In addition, the omega angle varies between -7gon and +4gon and phi varies between -21gon and +24gon, which allows to test the correctness of the used Formulas more thoroughly.

#	X0 [m]	Y0 [m]	Z0 [m]	$\omega$ [gon]	$\phi$ [gon]	$\kappa$ [gon]
1	-0.045	0.106	7.614	-0.626	-9.677	99.739
2	-0.045	0.105	7.615	-0.659	-9.703	199.764
3	-0.045	0.105	7.615	-0.594	-9.751	299.768
4	-0.045	0.106	7.614	-0.599	-9.756	399.719
5	-0.083	0.111	7.630	3.887	24.310	398.383
6	-0.083	0.110	7.630	3.871	24.263	298.414
7	-0.084	0.111	7.631	3.786	24.267	198.503
8	-0.084	0.110	7.630	3.843	24.343	98.374
9	-0.026	0.110	7.629	2.823	-21.465	98.077
10	-0.026	0.109	7.629	2.769	-21.501	198.010
11	-0.026	0.109	7.629	2.841	-21.518	298.046
12	-0.025	0.110	7.630	2.847	-21.475	397.913
13	-0.075	0.095	11.496	-7.343	1.040	0.051
14	-0.075	0.095	11.496	-7.334	0.979	300.071
15	-0.075	0.095	11.496	-7.430	0.952	200.120
16	-0.075	0.095	11.496	-7.385	1.128	100.005

Table 6. Exterior orientation parameters for an image subset.

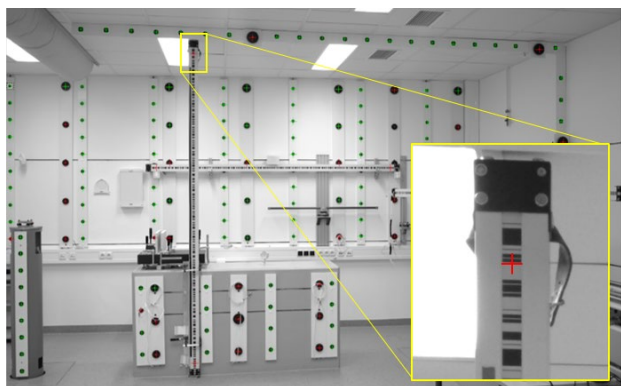


Figure 8. Vertical and horizontal level rods installed in the lab.

For later comparison, the 3D coordinates of the top (T) and bottom (B) reference points of the horizontal and vertical level bar have been derived by photogrammetric bundle adjustment (see Table 7). Those coordinates are also needed to determine the position and orientation of the level rods as they have not been surveyed after installation. In order to use Formulas (3), (4), (5) and (6), only the Z value is needed. However, a constant Z value is assumed for the level rods, which means that their normal vector needs to be aligned with the Z-axis of the lab.

This is the case for the vertical but unfortunately not for the horizontal level rod mounted on the back wall (see Figure 8). This is because the back wall of the lab is not strictly orthogonal

to the sidewall of the lab which can also be seen from the Z values of the top and bottom reference points which differ by about 15cm. To correct for this misalignment, the lab coordinate system is rotated by 3.13 deg around the Y-axis and the exterior orientation parameters are corrected accordingly (only for evaluation of the horizontal level).

As it can also be seen from the basic Equations (1) and (2), refined image coordinates have to be used. Measured image coordinates are therefore corrected for image distortion and principle point offset. From that, it is clear that the proposed validation not only covers the inner orientation but also the distortion parameters and thus the full set of calibration parameters.

In a rectified image, the level rod is depicted as a straight line between the upper and lower reference point. For evaluation of the 2D and 3D length, the line has been divided into sections of 1e-6 mm length to evaluate (9) and (10) for images where both reference points are visible. Enlarging the section length to 1e-4 mm did not change the 3D length significantly.

### 3.3 Results

As mentioned above, 3D coordinates of the reference points have been derived by photogrammetric reconstruction. It can be seen from Table 7 below that the estimated standard deviation  $sX$ ,  $sY$  and  $sZ$  numbers are also given with  $sZ$  being significantly larger as expected due to the limited camera baselines.

Level Rod	Pos	X [m] sX [mm]	Y [m] sY [mm]	Z [m] sZ [mm]	L <sub>3D</sub> [mm] sL [mm]
Horizontal	T	-0.8438 ±0.11	0.3862 ±0.11	0.4286 ±0.71	2800.38 ±1.1
	B	1.9524 ±0.22	0.3880 ±0.13	0.5817 ±0.76	
Vertical	T	-0.3203 ±0.09	1.3478 ±0.12	2.1664 ±0.49	2800.40 ±0.7
	B	-0.3222 ±0.10	-1.4526 ±0.14	2.1645 ±0.45	

Table 7. Level bar length measurements derived by 3D reconstruction of the top (T) and bottom (B) reference points.

From the 3D coordinates, the 3D length between the reference points is derived (see last column) together with its standard deviation. The deviation from the calibrated length of about 0.4mm is not significant due to the large standard deviation, which allows validation of the relative accuracy only up to ~1:3000. For the new method, we get results shown in Table 8 and 9.

Img#	H [m]	m <sub>s</sub> (T) [ ]	m <sub>s</sub> (B) [ ]	L <sub>2D</sub> [mm]	L <sub>3D</sub> [mm]
1	7.131	132.534	143.075	20.336	2800.333
2	7.132	132.505	143.090	20.336	2800.221
3	7.131	132.454	143.121	20.339	2800.287
4	7.131	132.443	143.118	20.339	2800.155
10	7.145	115.591	144.960	21.631	2799.980
12	7.146	115.643	144.974	21.625	2800.074
13	11.009	214.160	206.511	13.315	2800.145
14	11.008	214.143	206.594	13.313	2800.204
15	11.008	214.082	206.580	13.316	2800.227
16	11.008	214.166	206.368	13.319	2800.130

Table 8. Length measurements for the horizontal level rod.

Img#	H [m]	$m_s$ (T) [ ]	$m_s$ (B) [ ]	$L_{2D}$ [mm]	$L_{3D}$ [mm]
1	5.449	103.194	104.239	26.999	2800.190
2	5.449	103.163	104.264	26.999	2800.158
3	5.449	103.195	104.186	27.006	2800.241
4	5.449	103.184	104.183	27.006	2800.057
5	5.465	102.445	96.343	28.185	2800.059
6	5.465	102.461	96.392	28.179	2800.460
7	5.465	102.424	96.476	28.169	2800.174
8	5.465	102.403	96.371	28.188	2800.212
10	5.464	99.895	95.426	28.677	2799.905
12	5.464	99.964	95.367	28.679	2800.163
13	9.330	173.129	185.570	15.622	2800.100
14	9.330	173.137	185.563	15.622	2800.077
15	9.330	172.997	185.583	15.627	2799.977
16	9.330	173.068	185.579	15.624	2799.986

Table 9. Length measurements for the vertical level rod.

Measurements are given for the horizontal and vertical level rod for all images containing both reference points. The distance  $H$  between the camera and the level is given as well as the local scale  $m_s$  for the starting (top) and end point (bottom).  $L_{2D}$  is the length of the image line and  $L_{3D}$  the length computed in object space.

From the individual length measurements, the mean value  $L_M$  and standard deviation  $sL_M$  has been calculated for both level rods (see Table 10). The standard deviation for the vertical level rod is slightly lower due to the higher number of images used.

Level rod	$L_M$ [mm]	$sL_M$ [mm]	$L_M / sL_M$ [ ]
Horizontal	2800.126	$\pm 0.13$	1: 21.538
Vertical	2800.176	$\pm 0.10$	1: 28.000

Table 10. Statistical evaluation of the length measurements.

There seems to be no significant deviation from the calibrated length (2800.029 mm  $\pm 2\mu\text{m}$ ), at least for the horizontal level rod. As expected, the standard deviation  $sL_M$  is much lower (by a factor of ten) compared to the result of the 3D reconstruction (see Table 7). Dividing the standard deviation by the calibrated length, we get an indication of the relative accuracy achieved for this validation ( $\sim 1:25.000$ ). Such an accuracy would allow e.g. to detect a scale error caused by a deviation of  $2\mu\text{m}$  for the 50mm lens.

#### 4. Conclusions

For geometric calibration of digital aerial cameras lab calibration using a 3D test field is still the standard method. Phase One goes one step further and is not using precisely surveyed markers any more nor a temperature stabilized calibration room. Using a fully automated calibration workflow with very high redundancy, all lens types (50mm to 150mm) can be calibrated at a high accuracy level which has been cross checked by JOANNEUM RESEARCH using different software tools and doing calibration experiments with two Phase One reference cameras in Graz.

For lab validation of a camera calibration, we propose a new method, which uses standard geodetic equipment and avoids problems that can arise during 3D point reconstruction. The new method therefore allows validation of 3D length measurement at a ten times higher significance level than the standard 3D reconstruction method.

We think that we can further improve the relative accuracy level reached in this first experiment. First, the level rods should be mounted more stable and need to be surveyed to get their position and orientation at highest possible accuracy. Secondly, the illumination of the bar code on the level rods needs to be improved. In addition, more of such rods could be installed at different distances and even longer rods would improve the relative accuracy.

#### Acknowledgements

This research was partly funded by Phase One A/S.

#### References

- Bethmann, F. & Luhmann, T., 2011: Kleinste-Quadrat-Zuordnung mit erweiterten geometrischen Transformationen. In: Zeitschrift für Photogrammetrie – Fernerkundung – Geoinformation, Heft 2/2011, S. 57 – 69. DOI: 10.1127/1432-8364/2011/0073.
- Brown, D.C., 1971: Close-range camera calibration. Photogrammetric Engineering 37(8), 855-866.
- Cramer, M., 2006: Calibration and validation of digital airborne cameras. In: Revue Francaise de Photogrammetrie et de Teledetection.
- Cramer, M., 2008: The EuroSDR Approach on Digital Airborne Camera Calibration and Certification, International Archives of Photogrammetry and Remote Sensing IAPRS 27(B4), pp. 1753-1758, Proceedings 21. ISPRS Congress, Beijing 2008, digitally published on CD, 6 pages.
- Cramer, M., Grenzdörffer, G. & Honkavaara, Eija., 2010: In situ digital airborne camera validation and certification—the future standard. International Archives of Photogrammetry, Remote Sensing and Spatial Information Sciences. 38.
- DIN 18740-4:2025-05, 2025: Photogrammetric products – Part 4: Requirements for airborne and spaceborne digital cameras.
- ISO 10360-13:2021(E), 2021: Geometrical product specifications (GPS) – Acceptance and reverification tests for coordinate measuring systems (CMS), Part 13: Optical 3D CMS.
- ISO/TS 19159-1, 2014: Geographic information — Calibration and validation of remote sensing imagery sensors and data — Part 1: Optical sensors.
- Kresse, W., 2010: Development of an international standard for calibration and validation of remote sensing imagery sensors and data. International Archives of Photogrammetry, Remote Sensing and Spatial Information Sciences. 38
- Ladstädter, R., Gutjahr, K., Perko, R., Roncelli, D., Woschitz, H., 2025: Untersuchungen zur Kalibrierung und Validierung von Messkameras im Labor. In: Tagungsband der 23. Internationalen Geodätischen Woche Obergurgl, 215-227.
- Luhmann, T., 2023: Nahbereichsphotogrammetrie, 815 pages, ISBN 978-3-87907-732-8.

Maset, E., Fusiello, A., 2024: Scales of oblique photographs updated, *ISPRS Journal of Photogrammetry and Remote Sensing*, Band 207, 198-202.

Remondino, F., Fraser, C., 2005: Digital camera calibration methods: Considerations and comparisons, *ISPRS Commission V Symposium 'Image engineering and Vision Metrology'*, *IAPRS Volume XXXVI, Part 5, Dresden 25-27.9.2006*.

Stensaas, G. & Lee, G., 2008: Driving towards a worldwide acceptance procedure for digital airborne sensors, in *Proceedings of the XXI Congress of The International Society for Photogrammetry and Remote Sensing*.

VDI/VDE 2634 Blatt 1, 2002: *Optische 3D – Messsysteme – Bildgebende Systeme mit punktförmiger Antastung*, Verein Deutscher Ingenieure (VDI).